

Synthesis and characterization of ternary clusters containing the $[\text{As}_{16}]^{10-}$ anion, $[\text{MM}'\text{As}_{16}]^{4-}$ ($\text{M} = \text{Nb, Ta, M}' = \text{Cu, Ag}$)

Wei-Qiang Zhang^a, Harry W. T. Morgan^b, Cong-Cong Shu^a, John E. McGrady^{b,*}, and Zhong-Ming Sun^{a,*}

a. State Key Laboratory of Element-Organic Chemistry, Tianjin Key Lab for Rare Earth Materials and Applications, School of Materials Science and Engineering, Nankai University, Tianjin 300350, China.

b. Department of Chemistry, University of Oxford, South Parks Road, Oxford OX1 3QR, UK.

ABSTRACT: The $[\text{Nb@As}_8]^{3-}$ anion was first isolated from solution in 1986, and a number of isostructural $[\text{M@Pn}_8]^{n-}$ ($\text{M} = \text{Nb, Cr, Mo}$; $\text{Pn} = \text{As, Sb}$; $n=2, 3$) have since been reported. We show here how anions of this class can be used as synthetic precursors which, in combination with sources of low-valent late transition metals (Cu and Ag), generate ternary polyarsenide cluster anions with unprecedented structural motifs. The chain type $[\text{MM}'\text{As}_{16}]^{4-}$ ($\text{M} = \text{Nb, Ta}$; $\text{M}' = \text{Cu, Ag}$) units found in compounds **2-5**. These clusters contain a nortricyclane-like As_7 cage and a $[\text{M@As}_8]$ crown, linked by a single As atom, and so represents a fusion of two quite distinct branches of polyarsenide chemistry. Our analysis of the electronic structure confirms that the cluster retains many of the features of the component units. ESI-MS reveals a series of smaller component ions containing 8-12 As atoms, the DFT-computed structures of which can be understood in terms of the pseudo-element concept. This work not only exhibits a new type of coordination mode for As clusters but also offers a point of entry for rational design of multinary arsenic-based materials.

INTRODUCTION

The preparation of arsenic building blocks that can be used to generate materials with atomic precision and tunable physical and chemical properties remains a very significant challenge.^{1,2} The $[\text{As}_7]^{3-}$ unit (Figure 1a) is by far the most common arsenic source in this chemistry, and its reactions with transition-metal-based reagents have generated a range of binary polyarsenide clusters. This includes cases³⁻⁷ such as $[\text{As}_7\text{M}(\text{CO})_3]^{3-}$ ($\text{M} = \text{Cr, Mo, W}$), and $[\text{MAS}_{14}]^{4-}$ ($\text{M} = \text{Zn, Cd, Au}$), where the $[\text{As}_7]^{3-}$ cluster anion remains intact after coordination to the metal, but also examples such as $[\text{Co}(\eta^3\text{-As}_3)\{\eta^4\text{-As}_4(\text{Mes})_2\}]^{2-}$, $[\text{As}_{11}]^{3-}$ (Figure 1c), $[\text{EAs}_{15}]^{3-}$ ($\text{E} = \text{Sn, Hg, Zn}$, Figure 1b), and the 'Matryoshka cluster' $[\text{As@Ni}_{12}\text{@As}_{20}]^{3-}$ (Figure 1d), where the $[\text{As}_7]^{3-}$ unit undergoes extensive fragmentation and/or reconstruction.⁸⁻¹³ Whilst these and other arsenic compounds are generally toxic, they remain of considerable interest in catalysis, battery applications, medicine and especially in semiconductor devices.¹⁴⁻¹⁶

The synthesis of the one-dimensional polymer chain $[\text{RbNbAs}_8]^{2-}$ by von Schnering and co-workers in 1986 offers an alternative route into arsenic cluster chemistry based on the "inorganic ligands", $[\text{ME}_8]^{n-}$.¹⁷ The $[\text{As}_8]^{8-}$ crown is isoelectronic with S_8 and Se_8 , and coordinates to the metal in a D_{4d} -symmetric arrangement. The ability of these anions to selectively bind large alkali cations provides a simple model for cation binding in biologically-relevant cryptands. Eichhorn and co-workers have further extended the coordination chemistry of the $[\text{E}_8]^{8-}$ anions in a series of polypnictide complexes including $[\text{KCrAs}_8]^{2-}$

and $[\text{ME}_8]^{n-}$ ($\text{M} = \text{Nb, Cr, Mo}$; $\text{E} = \text{As, Sb}$; $n=2, 3$), all of which have been isolated through solution reactions.^{18,19} Computational work suggests that complexes of the group 7 metals (Mn, Tc, Re ; $n=3, 2, 1$) may also be stable²⁰, although this prediction is yet to be realised synthetically.

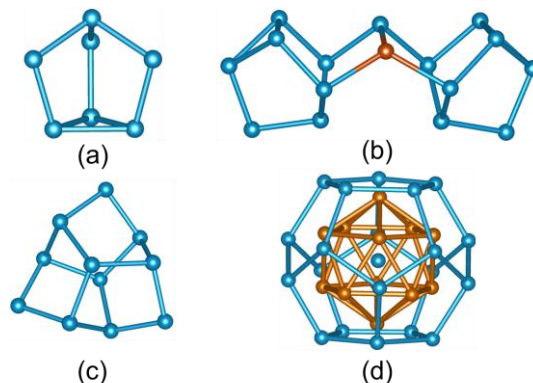


Figure 1. Structure of selected polyarsenic clusters with (a) $[\text{As}_7]^{3-}$, (b) $[\text{EAs}_{15}]^{3-}$ ($\text{E} = \text{Sn, Hg, Zn}$), (c) $[\text{As}_{11}]^{3-}$, (d) $[\text{As@Ni}_{12}\text{@As}_{20}]^{3-}$.

In this paper, we explore the potential of the $[\text{ME}_8]^{n-}$ unit to act as a synthetic precursor, providing access to ternary $\text{M}_x\text{M}'_y\text{As}_z$ clusters through reactions with transition-metal based reagents, precisely analogous to the reactions with $[\text{As}_7]^{3-}$. The accessibility of the $[\text{ME}_8]^{n-}$ unit across a wide range of transition metals and group 15 elements (As, Sb) makes it an attractive starting material for further synthetic chemistry, offering as it does a tool to control the $\text{M}:\text{E}$ ratio. Specifically, we report the synthesis and

characterization of the previously unknown Ta analogue of $[\text{Nb}@\text{As}_8]^{3-}$, $[\text{Ta}@\text{As}_8]^{3-}$, and the products of the reactions of $[\text{Nb}@\text{As}_8]^{3-}$ and $[\text{Ta}@\text{As}_8]^{3-}$ with $[\text{CuMes}(\text{PPh}_3)_2]\cdot\text{tol}$ and $[\text{AgMes}]_4$, both of which act as organometallic sources of low-valent late transition metals. The reactions with group 11 ($\text{M}' = \text{Cu}, \text{Ag}$) compounds lead to clusters with $\text{M}:\text{M}':\text{As}$ ratios of 1:1:16, in which two $[\text{As}_8]^{8-}$ ring fragments are oxidized to form a single contiguous $[\text{As}_{16}]^{10-}$ ligand.

EXPERIMENTAL PROCEDURES

All manipulations and reactions were performed under an inert atmosphere using standard Schlenk-line and/or glove-box techniques. Ethylenediamine (en, Aldrich, 99%), N, N-Dimethylformamide (Aldrich, 99.8%) and toluene (Aldrich, 99.8%) were distilled over sodium metal, CaH_2 and sodium/benzophenone, respectively, and were stored in gas-tight ampoules under nitrogen. $[\text{2.2.2}]\text{crypt}$ (4,7,13,16,21,24-Hexaoxa-1,10-diazabicyclo [8.8.8] hexacosane (Sigma-Aldrich, 98%) and triphenylphosphine (PPh_3 , Sigma-Aldrich, 99%) were dried in a vacuum for 12 h before use. The precursors of $[\text{CuMes}(\text{PPh}_3)_2]\cdot\text{tol}$, NbMes_2 , and $[\text{AgMes}]_4$ ($\text{Mes} = 1,3,5\text{-trimethylphenyl}$) were synthesized according to reported literature procedures.^{21,22} The solid-state phases K_7NbAs_4 and K_7TaAs_4 were prepared according to the reported literature.²³

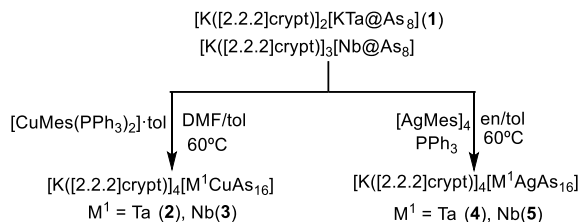
Synthesis of $[\text{K}([\text{2.2.2}]\text{crypt})]_3[\text{Nb}@\text{As}_8]^{24-}$:

K_7NbAs_4 (54 mg, 0.078 mmol) and $[\text{2.2.2}]\text{crypt}$ (120 mg, 0.32 mmol) were weighed into a 10 mL vial inside a glovebox and dissolved in 3 mL of ethylenediamine (en). NbMes_2 (14 mg, 0.04 mmol) was dissolved in toluene (0.5 mL) in a separate vial, producing a purple solution. The contents of the two vials were then mixed, yielding a red-brown solution. The reaction mixture was stirred for 3 h at 55°C and filtered through tightly-packed glass wool and transferred to a test tube, then carefully layered with toluene (4 mL) to allow for crystallization. Red crystals formed in the reaction vessel after 7 days in ~34% yield, 25.7 mg (based on the amount of K_7NbAs_4 used).

Synthesis of $[\text{K}([\text{2.2.2}]\text{crypt})]_2[\text{KTa}@\text{As}_8]$ (1):

K_7TaAs_4 (75 mg, 0.1 mmol), $[\text{2.2.2}]\text{crypt}$ (135 mg, 0.36 mmol), and PPh_3 (80 mg, 0.4 mmol) were weighed into a 10 mL vial inside a glovebox, dissolved in 3 mL of en and then stirred for 3 h at room temperature to yield a red-brown solution. The resulting solution was filtered through glass wool and transferred to a test tube, then carefully layered by toluene (4 mL) to allow for crystallization. After 12 days, large red-brown block-like crystals of $[\text{K}([\text{2.2.2}]\text{crypt})]_2[\text{KTa}@\text{As}_8]$ were observed on the bottom and wall of the test tube in ~33% yield, 27.2 mg (based on the amount of K_7TaAs_4 used).

The synthesis of compounds 2-5 from either $[\text{K}([\text{2.2.2}]\text{crypt})]_3[\text{Nb}@\text{As}_8]$ or $[\text{K}([\text{2.2.2}]\text{crypt})]_2[\text{KTa}@\text{As}_8]$ (1) is summarized in Scheme 1.



Scheme 1. Synthetic scheme of complexes 2-5. Mes = 1,3,5-trimethylphenyl, en = ethane-1,2-diamine, tol = toluene. All reaction solutions additionally contained $[\text{2.2.2}]\text{crypt} = 4,7,13,16,21,24\text{-hexaoxa-1,10-diazabicyclo [8.8.8] hexacosane}$.

Synthesis of $[\text{K}([\text{2.2.2}]\text{crypt})]_4[\text{TaCuAs}_{16}]$ (2).

Two methods were used to synthesize compound 2. **Method 1:** K_7TaAs_4 (60 mg 0.08 mmol) was weighed into a 10 mL vial inside a glovebox and dissolved in 3 mL of en. After stirring for thirty minutes, the resulting brown solution was filtered onto a toluene (1mL) solution of a mixture of $[\text{CuMes}(\text{PPh}_3)_2]\cdot\text{tol}$ (32 mg, 0.04 mmol) and $[\text{2.2.2}]\text{crypt}$ (132 mg, 0.35 mmol) and allowed to stir for a further three hours at 50 °C. The resulting red-brown solution was filtered through glass wool and transferred to a test tube, then carefully layered by toluene (5 mL) to allow for crystallization. Small Red-brown block-like crystals of $[\text{K}([\text{2.2.2}]\text{crypt})]_4[\text{TaCuAs}_{16}]$ (2) were isolated in relatively low yield ~20%, 12.4 mg (based on the amount of K_7TaAs_4 used).

Method 2: 50 mg, 0.03 mmol of pre-formed 1, $[\text{K}([\text{2.2.2}]\text{crypt})]_2[\text{KTa}@\text{As}_8]$ was dissolved in 2 mL of DMF along with $[\text{2.2.2}]\text{crypt}$ (10 mg, 0.03 mmol) and $[\text{CuMes}(\text{PPh}_3)_2]\cdot\text{tol}$ (32 mg, 0.04 mmol). The mixture was stirred for 2 h at 60 °C, yielding a dark brown solution which was filtered through glass wool and transferred to a test tube, then carefully layered by toluene (3 mL) to allow for crystallization. After 10 days, red-brown block-like crystals of compound 2 formed on the wall of the test tube in ~36 % yield, 16.8 mg (based on the amount of $[\text{K}([\text{2.2.2}]\text{crypt})]_2[\text{KTa}@\text{As}_8]$ used).

Synthesis of $[\text{K}([\text{2.2.2}]\text{crypt})]_4[\text{NbCuAs}_{16}]\cdot\text{DMF}$ (3)

50 mg, 0.025 mmol of $[\text{K}([\text{2.2.2}]\text{crypt})]_3[\text{Nb}@\text{As}_8]$ was dissolved in 2 mL of N, N-Dimethylformamide (DMF) solution and stirred for 10 min at room temperature to yield a red-brown solution. In another vial, $[\text{CuMes}(\text{PPh}_3)_2]\cdot\text{tol}$ (32 mg, 0.04 mmol) was dissolved in 0.5 mL tol and then added to the solution of $[\text{K}([\text{2.2.2}]\text{crypt})]_3[\text{Nb}@\text{As}_8]$. The reaction mixture was stirred for 3 h at 60 °C, yielding a red-brown solution which was filtered through glass wool and transferred to a test tube, then carefully layered by toluene (3 mL) to allow for crystallization. After 16 days, red-brown block-like crystals of $[\text{K}([\text{2.2.2}]\text{crypt})]_4[\text{NbCuAs}_{16}]\cdot\text{DMF}$ were observed in the bottom and the wall of the test tube in ~ 30% yield, 11.6 mg (based on the amount of $[\text{K}([\text{2.2.2}]\text{crypt})]_3[\text{Nb}@\text{As}_8]$ used).

Synthesis of $[\text{K}([\text{2.2.2}]\text{crypt})]_4[\text{TaAgAs}_{16}]$ (4).

Note: As organometallic silver compounds are sensitive to light, all processes should be performed in a dark environment unless otherwise noted. The vials and test tubes were wrapped in aluminum foil during the reaction and throughout the crystallization process.

[K([2.2.2]crypt)]₂[KTa@As₈] (50 mg, 0.03 mmol) and [2.2.2]crypt (10 mg, 0.03 mmol) were weighed into a 10 mL brown vial inside a glovebox and dissolved in 2.5 mL of ethylenediamine solution. [AgMes]₄ (32 mg, 0.03 mmol) and PPh₃ (10 mg, 0.038 mmol) were dissolved in 0.5 mL toluene solution in another brown vial, and then added dropwise to the solution of [K([2.2.2]crypt)]₂[KTa@As₈]. The reaction mixture was stirred for 2 h at 60 °C, yielding a brown solution that was filtered through glass wool and transferred to a test tube, then carefully layered by toluene (3 mL). After 30 days, red-brown block-like crystals of [K([2.2.2]crypt)]₄[TaAgAs₁₆] isolated in ~31% yield, 14.6 mg (based on the amount of [K([2.2.2]crypt)]₂[KTa@As₈] used).

Synthesis of [K([2.2.2]crypt)]₄[NbAgAs₁₆] (5)

The synthesis of **5** follows a very similar protocol to that described above for **4**. [K([2.2.2]crypt)]₃[Nb@As₈] (50 mg, 0.025 mmol) and [2.2.2]crypt (10 mg, 0.03 mmol) were dissolved in 2.5 mL of ethylenediamine in a 10 mL brown vial inside a glovebox. [AgMes]₄ (32 mg, 0.03 mmol) and PPh₃ (10 mg, 0.038 mmol) were dissolved in 0.5 mL toluene solution in a separate brown vial and added dropwise to the solution of [K([2.2.2]crypt)]₃[Nb@As₈]. The reaction mixture was stirred for 2 h at 60 °C, yielding a dark brown solution that was filtered through glass wool and transferred to a test tube, then carefully layered by toluene (3 mL). After 24 days, black block-like crystals of [K([2.2.2]crypt)]₄[NbAgAs₁₆] isolated in ~34% yield, 13 mg. (based on the amount of [K([2.2.2]crypt)]₃[Nb@As₈] used).

Single crystal X-ray Diffraction:

Suitable crystals of **1-5** were selected for X-ray diffraction analysis. Crystallographic data were collected on the Rigaku XtalAB Pro MM007 DW diffractometer with graphite monochromated Cu K α radiation (λ = 1.54184 Å). The structures of crystals **1-5** were solved using direct methods and then refined using SHELXL-2014 and Olex2.²⁵ All the non-hydrogen atoms were refined anisotropically, except for those in the split positions. The uncoordinated solvent molecules in complexes could not be modeled properly, so the solvent molecules are removed using Solvent Mask in Olex2. In compounds **2-5**, the cluster anion and sequestering agents ([2.2.2]crypt) have disordered structures, which were resolved using the mSplit process. A summary of the crystallographic data for the title compounds is listed in Supplementary Table S1, and selected bond distances and bond angles are given in Supplementary Table S2-6. CCDC entries 2058059 (**1**), 2058060 (**2**), 2039934 (**3**), 2077130 (**4**), and 2116761 (**5**) for compounds **1-5** contain the supplementary crystallographic data for this paper. These data can be obtained free of charge from the Cambridge Crystallographic Data Centre (www.ccdc.cam.ac.uk/data_requested/cif).

Electrospray Ionization Mass Spectrometry (ESI-MS) Investigations:

Negative ion mode ESI-MS of MeCN solutions made up from single crystals of **3** and **4** were measured on an LTQ linear ion trap spectrometer by Agilent Technologies ESI-TOF-MS (6230). The spray voltage was 5.48 kV and the

capillary temperature was maintained at 300 °C. The capillary voltage was 30 V. The samples were made up inside a glovebox under a nitrogen atmosphere and rapidly transferred to the spectrometer in an airtight syringe by direct infusion with a Harvard syringe pump at 0.2 mL/min.

Energy Dispersive X-ray (EDX) Spectroscopic Analysis:

EDX analysis on the title compound was performed using a scanning electron microscope (FE-SEM, JEOL JSM-7800F, Japan). Data acquisition was performed with an acceleration voltage of 15 kV and an accumulation time of 120 s.

Quantum chemical methods:

All calculations described in this paper were performed with the Amsterdam Density Functional (ADF) package of program, version 2020.103.^{26,27} For all geometry optimizations, a triple-zeta quality basis set of Slater-type orbitals was used, supplemented by a single set of polarization functions. Electrons up to and included 2p (Cu), 3d (Nb), 4d (Ta), 3p (As), and 2p (P) were treated using the frozen core approximation.²⁸ All calculations use the gradient-corrected approximations to the exchange-correlation functional proposed by Perdew, Burke, and Ernzerhof (PBE),²⁹ with a 'verygood' setting for the quality of the numerical integration. Scalar relativistic effects were included using the Zeroth order relativistic approximation (ZORA).³⁰ Vibrational frequencies were computed analytically, and all reported stationary points were confirmed to be minima through the absence of imaginary frequencies. The confining effect of cations in the solid state were simulated by using a continuum solvent model (COSMO) with a dielectric constant of ϵ_r = 78.39.³¹ The gradient algorithm of Versluis and Ziegler was employed in all geometry optimizations.³² The search for local minima for the ions observed in the ESI-MS was guided by two strategies. First, the pseudo-element concept, which identifies plausible connectivities for the As_x unit, was used to clusters with appropriate connectivity. In addition, 10,000 structures of a given stoichiometry were generated by placing the required number of atoms in a 5 x 5 x 5 Å box. These were then filtered to remove those with bond lengths shorter than 2.0 Å, and those where one or more atom was disconnected from the remainder of the cluster (all bond lengths > 2.8 Å), leaving 10-15 starting structures which were optimized using the protocol identified above. The reported structures represent the lowest energy minima identified by these two approaches combined.

RESULTS AND DISCUSSION

Structural chemistry.

Red-brown block-shaped crystals of [K([2.2.2]crypt)]₂[KTa@As₈] (**1**) were obtained using the solid-state Zintl phase K₇TaAs₄ as a precursor, as described in *Experimental Methods*. The structure of the anionic component of **1**, [KTa@As₈]²⁻, is isomorphic to the previously reported [RbNbAs₈]²⁻ and [KCrAs₈]²⁻ anions, with an approximately D_{4d}-symmetric As₈ ring encapsulating the Ta^V ion. The distances between K⁺ and the eight As atoms (3.883 Å, av.) are marginally longer than those in [KCrAs₈]²⁻ (3.776 Å, av.), consistent with the different ionic radii of Ta^V vs Cr^V. The four products, **2**, **3**, **4**, and **5** crystallize in the monoclinic space group P2₁/n with a unit

cell containing one independent $[MM'As_{16}]^{4-}$ anion ($M = Nb, Ta$; $M' = Cu, Ag$), four $[K([2.2.2]crypt)]^+$ cations and, in the case of **3**, a single N, N-Dimethylformamide (DMF) solvent molecule. A representative example of the $[MM'As_{16}]^{4-}$ ($M = Nb, Ta$; $M' = Cu, Ag$) unit (from cluster **2**) is shown in Figure 2. For better visualization, different labels are used to distinguish the anionic cluster and the molecular compounds, the **2a-5a** represent the anionic cluster in

compounds **2-5**. The four anions are isostructural, and all four exhibit positional disorder over two sites with an occupation ratio of 91:9 for **2a**, 62:38 for **3a**, 80:20 for **4a**, and 82:18 for **5a**, respectively. The structures of the two distinct cluster geometries are similar, and only the main component is discussed here. A comparison of selected bond distances for **1a-5a**

Table 1. Comparison of selected bond distances (Å) of $[KTa@As_8]^{2-}$, and $[M^1M^2As_{16}]^{4-}$ ($M^1 = Ta, Nb$; $M^2 = Cu, Ag$) ions.

Cluster		As-As	M^1 -As	M^2 -As
$[Ta@As_8]^{2-}$	1a	2.454-2.455	2.625-2.634	
$[TaCuAs_{16}]^{4-}$	2a	2.373-2.532	2.577-2.774	2.382-2.505
$[NbCuAs_{16}]^{4-}$	3a	2.374-2.515	2.582-2.774	2.388-2.560
$[TaAgAs_{16}]^{4-}$	4a	2.372-2.538	2.576-2.806	2.574-2.647
$[NbAgAs_{16}]^{4-}$	5a	2.378-2.552	2.578-2.798	2.564-2.656

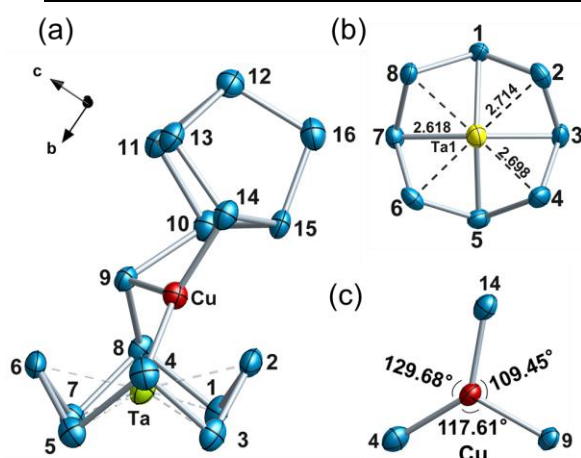


Figure 2. Structure of the anion $[TaCuAs_{16}]^{4-}$ (**2a**) with thermal ellipsoids at the 50% probability level. Key bond lengths of the $[M@As_8]^{n-}$ units in **2a** are included, as are the angles around Cu. The atoms are colored according to the following scheme: As = blue, Ta =lime, Cu = red.

is presented in Table 1 and a fuller summary of the metric parameters for all five clusters is given in Tables S2-S6. In all of **2a-5a**, the Nb^V/Ta^V center remains encapsulated in a crown-like As_8 ring, which is now connected to a separate As_7 unit via linking Cu/Ag and As atoms. The metal oxidation states, Cu/Ag^I and Nb/Ta^V suggest that the As_{16} ligand carries a formal charge of -10 , and indeed there are ten As vertices that are bonded to only two others, and therefore carry a formal negative charge according to the pseudo-element concept. The Cu/Ag center is coordinated by three of the As^- centers in an approximately trigonal planar array typical of Cu/Ag^I , (sum of angles: 356.75° (**2a**), 356.34° (**3a**), 359.95° (**4a**), and 359.92° (**5a**)). The Cu-As distances in all cases lie in the normal range (2.382–2.505 Å for **2a**, 2.388–2.560 Å for **3a**), and are similar to those in $[Cu_2As_{14}]^{4-}$ (2.435–2.490 Å) and the ‘*spiro*’ compound $\{[Cp''Fe(CO)_2]_2(\mu_3, \eta^{1:1:1:1}-As_4)\}_2Cu^+$ ($Cp'' = \eta^5-C_2H_2^tBu_3$) (2.456–2.499 Å).³³ The longest of these, the Cu-As4 distances (2.505(3) Å (**2a**), 2.560(3) Å (**3a**), respectively) are to the As atom in the As_8 ring, where proximity to the M^V center will reduce the charge density. The

average As-As bond lengths in the $[M@As_8]$ unit (2.472 Å for **2a**, 2.467 Å for **3a**, 2.470 Å for **4a**, and 2.484 Å for **5a**, respectively) are very similar to those in $[Nb@As_8]^{3-}$ (2.447 Å, av.) and $[Ta@As_8]^{3-}$ (2.454 Å, av.), while those within the As_7 unit (2.425 Å–2.438 Å) are very typical of nortricyclane-like $[MAS_7]^{3-}$ clusters.³⁴ In short, the fusion of the $[M@As_8]^{3-}$ and As_7^{3-} units in **3-5** appears to do little to perturb the intrinsic structure of either component.

The M:As ratio of 1:16 in the major products **2-5** compared to 1:8 in the $[M@As_8]^{3-}$ starting materials indicates that 50% of the Nb/Ta content is lost in the process of aggregation. We have not been able to characterize this missing content, but clearly de-coordination of the group 5 metal, along with release of ‘free’ As, occurs at some stage in the reaction. Moreover, the average As oxidation state of $-5/8$ in the products is lower than that in the starting material (-1), indicating that oxidation of As is integral to the reaction. It is possible that the group 5 metal ion is reduced during the reaction, although an alternative possibility is that the PPh_3 ligand released from the Cu starting material is the oxidizing agent. Whilst this phosphine is well known to act as a reducing agent (forming PPh_3O in the process), there is also precedent for it acting as an oxidizing agent in Zintl-ion chemistry, forming PPh_2^- in the process.^{35,36} In this context, we recall that it is also possible to synthesize **2**, albeit only in a low yield, from the direct reaction of the solid-state Zintl phase ‘ K_7TaAs_4 ’ with $[CuMes(PPh_3)_2] \cdot tol$ ($tol = toluene$) in the presence of DMF/[2.2.2]crypt (**Method 2** in Experimental methods). In this case a more oxidized form of As (As_7^{3-}) is already present in the reaction mixture, and so oxidative release of As from a group 5 complex is not required prior to fusion of the two component subunits.

The unique nature of the As_{16}^{10-} unit, combining as it does structural components that are typical of As in rather different oxidation levels (crown-like As_8^{8-} and nortricyclane-like As_7^{3-}) in the same compound prompted us to explore the electronic structure using density functional theory (PBE functional, triple-zeta+polarization quality basis, ADF2020 programme – full details are given in Experimental Methods).

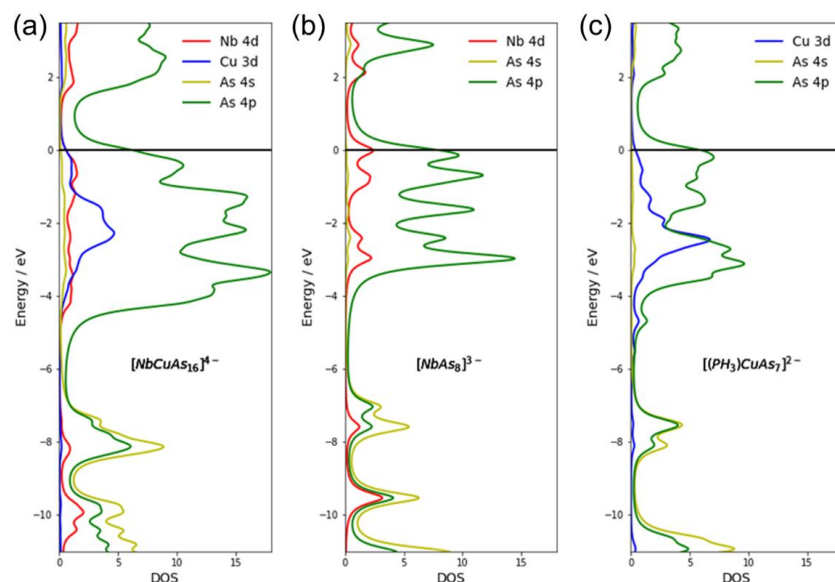


Figure 3. Projected densities of states for (a) $[\text{NbCuAs}_{16}]^{4-}$, (b) $[\text{Nb@As}_8]^{3-}$, and (c) $[(\text{PH}_3)\text{CuAs}_7]^{2-}$. The discrete molecular energy levels are broadened by a Lorentzian with full width at half maximum (FWHM) of 0.25 eV.

The $[\text{NbCuAs}_{16}]^{4-}$ cluster in **3** used as an illustrative example, but the electronic structure is very similar across all four compounds, **2-5**. As points of reference for the component parts of the cluster, we have also considered the $[\text{NbAs}_8]^{3-}$ cluster, the electronic structure of which has previously been described by Li and co-workers,²⁰ and also the $[\text{As}_7\text{Cu}(\text{PPh}_3)]^{2-}$ dianion³⁷ (where the Ph groups have been replaced by H for computational expedience). The densities of states generated by Lorentzian broadening (FWHM 0.25 eV) of the discrete molecular levels for the three molecules are compared in Figure 3. In all cases the position of the Fermi level ($E = 0$) is taken as the energy of the highest occupied molecular orbital (HOMO) of the complex. It is immediately striking that the DOS of $[\text{NbCuAs}_{16}]^{4-}$ is approximately the sum of the two components, and that the positions of the Cu 3d levels (in $[\text{NbCuAs}_{16}]^{4-}$ and $[(\text{PH}_3)\text{CuAs}_7]^{2-}$) and the Nb 4d levels (in $[\text{NbCuAs}_{16}]^{4-}$ and $[\text{NbAs}_8]^{3-}$) are almost coincident. The very similar span of the As 4p levels at and below the Fermi level (0 to -4.0 eV) in all three compounds suggests that the different oxidation levels of the component parts are largely formal, and that the electron densities at the As

centers in the As_8 and As_7 components of the cluster are largely equalized.

ESI-mass spectrometry and cluster fragmentation.

The negative-ion ESI mass spectrum of a crystalline sample of **4** ($[\text{K}([2.2.2]\text{crypt})]_4[\text{TaAgAs}_{16}]$) re-dissolved in MeCN is shown in Figure 4(a), with expanded views of key peaks shown in Figure 4(b). The corresponding spectrum of **3** ($[\text{K}([2.2.2]\text{crypt})]_4[\text{NbCuAs}_{16}]$) is presented in Supporting information, Figure S12, and shows very similar features. Prominent peaks in Figure 4(a) can be assigned to the parent ion in combination with either three (m/z 2734.423) or one (m/z 1903.8082) $[\text{K}([2.2.2]\text{crypt})]^+$ cation(s), along with less intense features due to the protonated form (m/z 1487.5987). The intensity of these peaks confirms that the As_{16} unit is robust enough to survive the ESI conditions, but the distribution of low-mass peaks (in the window m/z 750-850) offers an intriguing insight into the richness of As cluster chemistry following fragmentation. The most intense peak in this region is assigned to the $[\text{TaAgAs}_9]^-$ anion at m/z 962.1495, but there are also smaller peaks assigned to $[\text{TaAgAs}_{11}]^-$, and the Ag-free anions $[\text{TaAs}_8]^-$, $[\text{TaAs}_{10}]^-$ and $[\text{TaAs}_{12}]^-$.

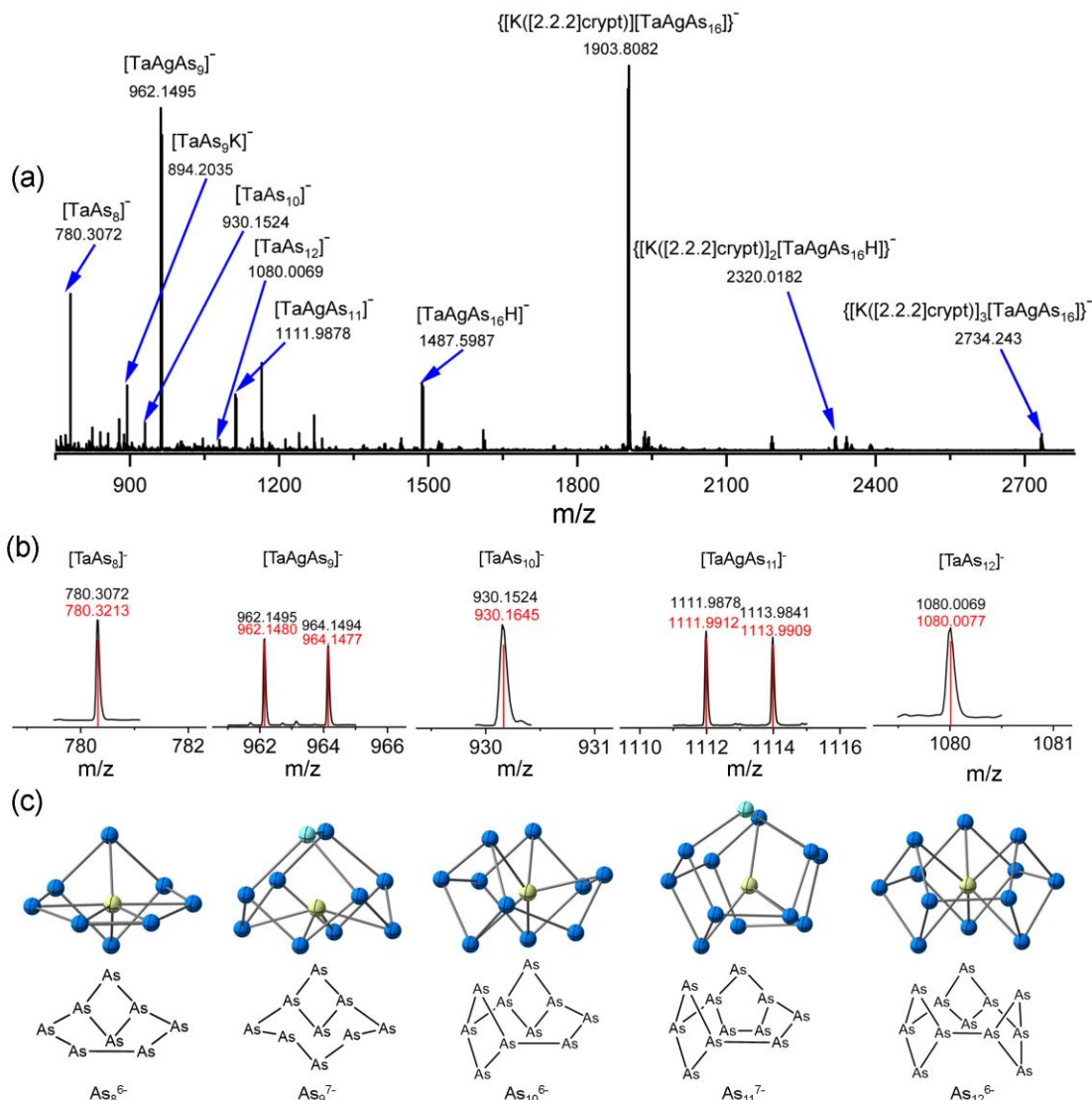


Figure 4. (a) Negative-ion ESI mass spectrum over the range of m/z 700–2400 of **4**. (b) Mass spectra of measured (black) and calculated (red) isotope patterns for selected low-mass peaks and (c) the optimized structure of the lowest-energy isomer is for the stated composition, along with a representation of the As_x^{n-} skeleton. The colours of atoms are as follow: Ag = turquoise, As = blue and Ta = yellow.

The As:Ta ratio across this series of mono-anions therefore goes from 8 all the way through to 12, with all members having an even electron count. The $[TaAs_{12}]^-$ case is particularly significant in that it is valence isoelectronic with the $[LaSb_{12}]^{3-}$ anion,³⁸ and our survey of the DFT potential energy surface indicates that the Ta compound adopts the same structure, based on three rhombic As_4^{2-} units linked by As–As single bonds to give a cyclic As_{12}^{6-} unit. The As_{10}^{6-} and As_8^{6-} ligands present in $[TaAs_{10}]^-$ and $[TaAs_8]^-$, respectively, can be straightforwardly understood in terms of sequential loss of pairs of As atoms from the $[TaAs_{12}]^-$ precursor, transformations that leave the number of As vertices that are bound to only two others unchanged at 6. The common 6– charge of the three As_x ligands is therefore consistent with the pseudo-element concept, where the two-connected vertices carry a formal negative charge. Similarly, the As_9^{7-} ligand in $[TaAs_9Ag]^-$ has only a single rhombic face, and seven of the nine vertices are connected to two others. This fragment is strikingly similar in struc-

ture to the corresponding unit in the crystal structure of $[TaAgAs_{16}]^{4-}$, the only significant difference being that the 9th As atom (As9 in Figure 2) is bonded to two members of the As_8 ring rather than only one. The As_{11}^{7-} ligand in $[TaAs_{11}Ag]^-$ is derived (at least conceptually) from the insertion of an additional As atom into one As_4 rhombus of $[TaAs_{10}]^-$ to form a pentagonal As_5 ring, the As_{11} unit again having seven two-connected vertices. Overall, then, the structural chemistry of the family of low-mass fragments observed in the ESI-MS can be understood entirely within the framework of the pseudo-element concept. The ligand expansion series shown in Figure 4(c) corresponds, at least in a formal sense, to the sequential addition either of ‘As[–]’ ($As_8^{6-} \rightarrow As_9^{7-}$, $As_{10}^{6-} \rightarrow As_{11}^{7-}$), which inserts into an existing As–As bond, or of ‘As⁺’ ($As_9^{7-} \rightarrow As_{10}^{6-}$, $As_{11}^{7-} \rightarrow As_{12}^{6-}$), which adds across the termini of an As_3 unit to form a rhombus. This series establishes a formal relationship between the various clusters based on electron count, but does not constitute a ‘mechanism’ of growth simply be-

cause the data is not resolved in any temporal sense. It is possible, for example, that the different clusters shown in Figure 4 are not formed by sequential gain/loss of As but rather by gain/loss of pairs of As atoms, or indeed from entirely different fragmentation pathways of the parent ion. Nevertheless, it is clear that the fragmentation products that dominate the low-mass region of the ESI-MS reflect stability patterns that can be understood in terms of simple valence concepts.³⁹

CONCLUSIONS

In summary, we have reported here the synthesis and characterization of four clusters that contain the contiguous As_{16}^{10-} ligand, a new member of the polyarsenide family. The two distinct components of the As_{16}^{10-} ligand display the characteristic coordination chemistry of their isolated analogues: the As_8 unit binds a high-valent transition metal ion ($\text{Nb}^{\text{V}}/\text{Ta}^{\text{V}}$) in the center of the ring, while also being able to bind an electronically inert mono-cation (Cu^+/Ag^+) on one As_4 face, just as K^+ and Rb^+ bind to $[\text{NbAs}_8]^{3-}$ and $[\text{CrAs}_8]^{3-}$, respectively in the 1-dimensional polymers. The negative ion ESI-MS of solutions of **3** and **4** show characteristic peaks due to the parent ions, but also a number of smaller peaks at lower mass arise from fragmentation of the As_{16}^{10-} ligand. Peaks corresponding to molecular species containing As_8^{6-} , As_9^{7-} , As_{10}^{6-} , As_{11}^{7-} and As_{12}^{6-} are all present, and in all cases the optimized geometries are consistent with expectations based on the pseudo-element concept.

ASSOCIATED CONTENT

Supporting Information

Crystallographic supplementary information, ESI-MS studies, Energy Dispersive X-ray (EDX) spectroscopic analysis and details of DFT-optimized energies and cartesian coordinates.

Accession Codes

CCDC entries 2058059 (**1**), 2058060 (**2**), 2039934 (**3**), 2077130 (**4**), and 2116761 (**5**) for compounds **1-5** contain the supplementary crystallographic data for this paper. These data can be obtained free of charge via www.ccdc.cam.ac.uk/data_request/cif

AUTHOR INFORMATION

Corresponding Author

Zhong-Ming Sun – State Key Laboratory of Elemento-Organic chemistry, Tianjin Key Lab for Rare Earth Materials and Applications, School of Materials Science and Engineering, Nankai University, Tianjin 300350, China; orcid.org/0000-0003-2894-6327; Email: sun-lab@nankai.edu.cn

John E. McGrady – Department of Chemistry, University of Oxford, South Parks Road, Oxford OX1 3QR, UK; orcid.org/0000-0002-8991-1921; E-mail: john.mcgrady@chem.ox.ac.uk

Authors

Wei-Qiang Zhang – State Key Laboratory of Elemento-Organic Chemistry, Tianjin Key Lab for Rare Earth Materi-

als and Applications, School of Materials Science and Engineering, Nankai University, Tianjin 300350, China; orcid.org/0000-0002-9301-529X

Harry W. T. Morgan – Department of Chemistry, University of Oxford, South Parks Road, Oxford OX1 3QR, UK;

Cong-Cong Shu – Tianjin Key Lab for Rare Earth Materials and Applications, State Key Laboratory of Elemento-Organic Chemistry, School of Materials Science and Engineering, Nankai University, Tianjin 300350, China; orcid.org/0000-0001-7407-3446

Notes

The authors declare no competing financial interest.

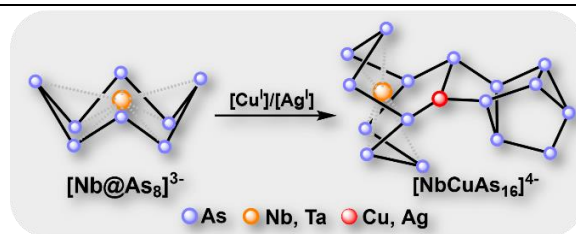
ACKNOWLEDGMENT

This work was supported by the National Natural Science Foundation of China (92161102, 21971118) and the Natural Science Foundation of Tianjin City (No. 20JCYBJC01560) to Z.-M.S. H.W.T.M. thanks the EPSRC for support through the Centre for Doctoral Training, Theory and Modelling in Chemical Sciences under Grant EP/L015722/1.

REFERENCES

- (1) Kang, J. S.; Li, M.; Wu, H.; Nguyen, H.; Hu, Y. Experimental observation of high thermal conductivity in boron arsenide. *Science* **2018**, *361*, 575–578.
- (2) Zhang, S.; Yan, Z.; Li, Y.; Chen, Z.; Zeng, H. Atomically thin arsenene and antimonene: semimetal-semiconductor and indirect-direct band-gap transitions. *Angew. Chem. Int. Ed.* **2015**, *54*, 3112–3115.
- (3) Eichhorn, B. W.; Haushalter, R. C.; Huffman, J. C. Insertion of $\text{Cr}(\text{CO})_3$ into As to form $[\text{As}_7\text{Cr}(\text{CO})_3]^{3-}$: An inorganic Nortricyclane-to-norbornadiene conversion. *Angew. Chem. Int. Ed.* **1989**, *28*, 1032–1033.
- (4) Kesanli, B.; Charles, S.; Lam, Y. F.; Bott, S. G.; Fetting, J.; Eichhorn, B. W. Probing individual steps of dynamic exchange with ^{31}P EXSY NMR spectroscopy: synthesis and characterization of the $[\text{E}_7\text{PtH}(\text{PPh}_3)]^{2-}$ Zintl ion complexes $[\text{E} = \text{P}, \text{As}]$. *J. Am. Chem. Soc.* **2000**, *122*, 11101–11107.
- (5) Mandal, S.; Reber, A. C.; Qian, M.; Liu, R.; Saavedra, H. M.; Sen, S.; Weiss, P. S.; Khanna, S. N.; Sen, A. Synthesis, structure and band gap energy of covalently linked cluster-assembled materials *Dalton Trans.* **2012**, *41*, 12365–12377.
- (6) Qian, M.; Reber, A. C.; Ugrinov, A.; Chaki, N. K.; Mandal, S.; Saavedra, H. M.; Khanna, S. N.; Sen, A.; Weiss, P. S. Cluster-assembled materials: toward nanomaterials with precise control over properties. *ACS Nano*. **2010**, *4*, 235–240.
- (7) Turbervill, R. S. P.; Goicoechea, J. M. From clusters to unorthodox pnictogen sources: solution-phase reactivity of $[\text{E}_7]^{3-}$ ($\text{E} = \text{P-Sb}$) anions. *Chem. Rev.* **2014**, *114*, 10807–10828.
- (8) Belin, C. H. E. Polyarsenide anions. Synthesis and structure of a salt containing the undecaarsenide($3-$) ion. *J. Am. Chem. Soc.* **1980**, *102*, 6036–6040.
- (9) Kaas, M.; Korber, N. Synthesis and characterization of $[\text{Rb}([18]\text{crown-6})]_3\text{As}_{15}\text{Zn}\cdot 4\text{NH}_3$ and $[\text{Rb}([2.2.2]\text{crypt})]_4\text{Sb}_{14}\text{Zn}\cdot 8\text{NH}_3$. *Z. Anorg. Allg. Chem.* **2017**, *643*, 1331–1334.
- (10) Hanauer, T. J.; Aschenbrenner, C.; Korber, N. Dimers of heptapnictide anions: As_{14}^{4-} and P_{14}^{4-} in the crystal structures of $[\text{Rb}([18\text{-crown-6}])_4\text{As}_{14}\cdot 6\text{NH}_3]$ and $[\text{Li}(\text{NH}_3)_4]_4\text{P}_{14}\cdot \text{NH}_3$. *Inorg. Chem.* **2006**, *45*, 6723–6727.
- (11) Moses, M. J.; Fetting, J.; Eichhorn, B. W. Charged molecular alloys: synthesis and characterization of the binary anions $\text{Pd}_7\text{As}_{16}^{4-}$ and $\text{Pd}_2\text{As}_{14}^{4-}$. *J. Am. Chem. Soc.* **2002**, *124*, 5944–5945.

- (12) Moses, M. J.; Fetting, J. C.; Eichhorn, B. W. Interpenetrating As₂₀ fullerene and Ni₁₂ icosahedra in the onion-skin [As@Ni₁₂@As₂₀]³⁻ ion. *Science* **2003**, *300*, 778–780.
- (13) Knapp, C. M.; Westcott, B. H.; Raybould, M. A. C.; McGrady, J. E.; Goicoechea, J. M. Transition-metal-mediated activation of the heptaarsenide trianion: isolation of a diaryltetraarsenabutadienediide. *Chem. Commun.* **2012**, *48*, 12183–12185.
- (14) Seidl, M.; Balazs, G.; Scheer, M. The Chemistry of Yellow Arsenic. *Chem. Rev.* **2019**, *119*, 8406–8434.
- (15) Blakemore, J. S. Semiconducting and other major properties of gallium arsenide. *J. Appl. Phys.* **1982**, *53*, R123–R181.
- (16) Grund, S. C.; Hanusch, K.; Wolf, H. U. Arsenic and Arsenic Compounds. In *Ullmann's Encyclopedia of Industrial Chemistry*; Ed.; Wiley, (2008). DOI: 10.1002/14356007.a03_113.pub2.
- (17) von Schnering, H. G.; Wolf, J.; Weber, D.; Ramirez, R.; Meyer, T. [NbAs₈]³⁻, a novel type of complex and an unexpected one-dimensional chain structure: [Rb{NbAs₈}]²⁻. *Angew. Chem. Int. Ed.* **1986**, *25*, 353–354.
- (18) Kesanli, B.; Fetting, J.; Eichhorn, B. W. Controlled aggregation of ME₈ⁿ⁻ binary anions (M = Cr, Mo; E = As, Sb) into one-dimensional arrays: structures, magnetism and spectroscopy. *J. Am. Chem. Soc.* **2003**, *125*, 7367–7376.
- (19) Eichhorn, B. W.; Mattamana, S. P.; Gardner, D. R.; Fetting, J. C. Synthesis, structure and coordination chemistry of [MoAs₈]²⁻. *J. Am. Chem. Soc.* **1998**, *120*, 9708–9709.
- (20) Li, J.; K. Wu, Electronic structures and properties of eight-coordinate metal-polyarsenic complexes MAs₈ⁿ⁻ (M = V, Nb, Ta, Cr, Mo, W, Mn, Tc, Re). *Inorg. Chem.* **2000**, *39*, 1538–1544.
- (21) Meyer, E. M.; Gambarotta, S.; Floriani, C.; Chiesi-Villa, A.; Guastini, C. Polynuclear aryl derivatives of Group 11 metals. Synthesis, solid state-solution structural relationship, and reactivity with phosphines. *Organometallics* **1989**, *8*, 1067–1079.
- (22) Calderazzo, F.; Pampaloni, G.; Rocchi, L. Synthesis and reactivity of η⁶-arene derivatives of niobium(II), niobium(I), and niobium(0). *J. Organomet. Chem.* **1991**, *413*, 91–109.
- (23) Nuss, J.; Gil, R. H. C.; Honle, W.; Peters, K.; von Schnering, H. G. Synthese, struktur und eigenschaften der tetraarsenidometallate(V) M₇[TAs₄] (M = K, Rb; T = Nb, Ta). *Z. Anorg. Allg. Chem.* **1996**, *622*, 1854–1864.
- (24) Kesanli, B.; Fetting, J.; Scott, B.; Eichhorn, B. W. Gas phase, solution, and solid-state alkali ion binding by the [NbE₈]³⁻ (E = As, Sb) Complexes: Synthesis, Structure, and Spectroscopy *Inorg. Chem.* **2004**, *43*, 3840–3846.
- (25) Dolomanov, O. V.; Bourhis, L. J.; Gildea, R. J.; Howard, J. A. K.; Puschmann, H. OLEX2: a complete structure solution, refinement and analysis program. *J. Appl. Cryst.* **2009**, *42*, 339–341.
- (26) te Velde, G.; Bickelhaupt, F. M.; Baerends, E. J.; Fonseca Guerra, C.; van Gisbergen, S. J. A.; Snijders, J. G.; Ziegler, T. Chemistry with ADF. *J. Comp. Chem.*, **2001**, *22*, 931–967.
- (27) ADF 2020, SCM, Theoretical Chemistry, Vrije Universiteit, Amsterdam, The Netherlands, <http://www.scm.com>
- (28) Lenthe, E. V.; Baerends, E. J. Optimized Slater-type basis sets for the elements 1–118. *J. Comp. Chem.* **2003**, *24*, 1142–1156.
- (29) Perdew, J. P.; Burke, K.; Ernzerhof, M. Generalized gradient approximation made simple. *Phys. Rev. Lett.* **1996**, *77*, 3865–3868.
- (30) (a) Lenthe, E. V.; Baerends, E. J.; Snijders, J. G. Relativistic regular two-component Hamiltonians. *J. Chem. Phys.* **1993**, *99*, 4597–4610; (b) Lenthe, E. V.; Baerends, E. J.; Snijders, J. G. Relativistic total energy using regular approximations. *J. Chem. Phys.*, **1994**, *101*, 9783–9792; (c) Lenthe, E. V.; Ehlers, A. E.; Baerends, E. J. Geometry optimizations in the zero order regular approximation for relativistic effects. *J. Chem. Phys.* **1999**, *110*, 8943–8953.
- (31) Pye, C. C.; Ziegler, T. An implementation of the conductor-like screening model of solvation within the Amsterdam density functional package. *Theor. Chem. Acc.* **1999**, *101*, 396–408.
- (32) Versluis, L.; Ziegler, T. The determination of molecular structures by density functional theory. The evaluation of analytical energy gradients by numerical integration. *J. Chem. Phys.* **1988**, *88*, 322–328.
- (33) Schwarzmaier, C.; Heint, S.; Balázs, G.; Scheer, M. E₄ Butterfly Complexes (E = P, As) as Chelating Ligands. *Angew. Chem. Int. Ed.* **2015**, *54*, 13116–13121.
- (34) Charles, S.; Eichhorn, B. W.; Rheingold, A. L.; Bott, S. G. Synthesis, structure, and properties of the [E₇M(CO)₃]³⁻ complexes where E = P, As, Sb and M = Cr, Mo, W. *J. Am. Chem. Soc.* **1994**, *116*, 8077–8086.
- (35) Ugrinov, A.; Sevov, S.; [Ge₉dGe₉dGe₉]⁶⁻: A Linear Trimer of 27 Germanium Atoms. *J. Am. Chem. Soc.*, **2002**, *124*, 10990–10991.
- (36) Sevov, S.; Goicoechea, J. M. Chemistry of deltahedral Zintl ions, *Organometallics*, **2006**, *25*, 5678–5692.
- (37) Zhang, W. Q.; Tkachenko, N. V.; Qiao, L.; Boldyrev, A. I.; Sun, Z. M. Synthesis and structure of binary copper/silver-arsenic clusters derived from Zintl ion As₇³⁻. *Chin. J. Chem.*, **2021**, *40*, 65–70.
- (38) Min, X.; Popov, I. A.; Pan, F. X.; Li, L.-J.; Matito, E.; Z.-M. Sun, Z.-M. S.; Wang, L.-S.; Boldyrev, A. I. All-metal antiaromaticity in Sb₄-type lanthanocene anions. *Angew. Chem., Int. Ed.*, **2016**, *55*, 5531–5535.
- (39) McGrady, J. E.; Weigend, F.; Dehnen, S. Electronic structure and bonding in endohedral Zintl clusters, *Chem. Soc. Rev.*, **2021**, in press.



A family of ternary heterometallic polyarsenide clusters, $[\text{MM}'\text{As}_{16}]^{4-}$ ($\text{M} = \text{Nb}, \text{Ta}$; $\text{M}' = \text{Cu}, \text{Ag}$), were obtained through the reaction of intermetalloid cluster, $[\text{M}@\text{As}_8]^{3-}$, and low valent group 11 metal salt. These compounds represent a link between the chemistry of the moderately reduced cage-like structures of $[\text{As}_7]^{3-}$ and the more highly reduced 2-connected rings typified by $[\text{M}@\text{As}_8]^{n-}$. This work not only exhibits a new type of coordination mode for As clusters but also offers a point of entry for rational design of multinary arsenic-based materials.
